View metadata, citation and similar papers at core.ac.uk

brought to you by CORE

provided by Longwood University

Longwood University
Digital Commons @ Longwood University

Chemistry and Physics Faculty Publications | Chemistry and Physics

1-1997

Comparison of the Projector Augmented-Wave, Pseudopotential, and Linearized Augmented-Plane-Wave Formalisms for Density-Functional Calculations of Solids

N. A. W. Holzwarth
Wake Forest University

G. E. Matthews
Wake Forest University

Rodney Dunning
Longwood University, dunningrb@longwood.edu

A. R. Tackett
Wake Forest University

Y. Zeng
Wake Forest University

Follow this and additional works at: http://digitalcommons.longwood.edu/chemphys_facpubs

 Part of the Physics Commons

Recommended Citation

Holzwarth, N. A. W.; Matthews, G. E.; Dunning, Rodney; Tackett, A. R.; and Zeng, Y., "Comparison of the Projector Augmented-Wave, Pseudopotential, and Linearized Augmented-Plane-Wave Formalisms for Density-Functional Calculations of Solids" (1997). *Chemistry and Physics Faculty Publications.* Paper 2.
http://digitalcommons.longwood.edu/chemphys_facpubs/2

This Article is brought to you for free and open access by the Chemistry and Physics at Digital Commons @ Longwood University. It has been accepted for inclusion in Chemistry and Physics Faculty Publications by an authorized administrator of Digital Commons @ Longwood University. For more information, please contact hinestm@longwood.edu.

Comparison of the projector augmented-wave, pseudopotential, and linearized augmented-plane-wave formalisms for density-functional calculations of solids

N. A. W. Holzwarth, G. E. Matthews, R. B. Dunning, A. R. Tackett, and Y. Zeng
Department of Physics, Wake Forest University, Winston-Salem, North Carolina 27109
(Received 8 July 1996)

The projector augmented-wave (PAW) method was developed by Blöchl as a method to accurately and efficiently calculate the electronic structure of materials within the framework of density-functional theory. It contains the numerical advantages of pseudopotential calculations while retaining the physics of all-electron calculations, including the correct nodal behavior of the valence-electron wave functions and the ability to include upper core states in addition to valence states in the self-consistent iterations. It uses many of the same ideas developed by Vanderbilt in his ''soft pseudopotential'' formalism and in earlier work by Blöchl in his ''generalized separable potentials,'' and has been successfully demonstrated for several interesting materials. We have developed a version of the PAW formalism for general use in structural and dynamical studies of materials. In the present paper, we investigate the accuracy of this implementation in comparison with corresponding results obtained using pseudopotential and linearized augmented-plane-wave (LAPW) codes. We present results of calculations for the cohesive energy, equilibrium lattice constant, and bulk modulus for several representative covalent, ionic, and metallic materials including diamond, silicon, SiC, CaF_2, fcc Ca, and bcc V. With the exception of CaF_2, for which core-electron polarization effects are important, the structural properties of these materials are represented equally well by the PAW, LAPW, and pseudopotential formalisms. [S0163-1829(97)00404-9]

I. INTRODUCTION

The ''projector augmented-wave'' (PAW) method was developed by Blöchl[1] as a method to accurately and efficiently calculate the electronic structure of materials within the framework of density-functional theory.[9,10] It takes advantage of many of the ideas developed in the pseudopotential literature,[11,12] while retaining information about the correct nodal behavior of the valence electron wave functions and has the ability to include upper core states in addition to valence states in the self-consistent iterations. It uses many ideas similar to those developed by Vanderbilt[2] in his ''soft pseudopotential'' formalism and by Blöchl[3] in his earlier work on ''generalized separable potentials,'' and has been successfully demonstrated for several interesting materials.[1,4–6]

We have developed a version of the PAW formalism for general use in structural and dynamical studies of materials. We have investigated this implementation as a function of computational parameters and in comparison with corresponding results obtained using pseudopotential [7,11,13] and linearized augmented-plane-wave[8] (LAPW) codes. The focus of this study is the numerical accuracy of the computational technique. Therefore, all calculations described in this work were done using the exchange-correlation functional in the local density approximation (LDA) parametrized by Perdew and Wang.[14] Extension of the current formalism to more complicated exchange-correlation functionals[15], or to include relativistic and/or spin effects, should be straightforward.

There are several motivations for developing the PAW formalism. A number of physical properties (such as magnetic properties, electronic matrix elements, for example) should be calculated with a knowledge of the correct nodal behavior of the valence electron wave functions. In addition, there is evidence that it is sometimes necessary to improve upon the accuracy of the pseudopotential approach for the structural simulations of some materials.

Within the framework of density-functional theory,[9,10] pseudopotential methods have been enormously successful in performing structural studies of a wide variety of materials.[11,12] One contributing factor to this success is the accuracy of the frozen core approximation[16] for many of the materials throughout the Periodic Table. In order to get a more quantitative assessment of the accuracy of the frozen core approximation, it is helpful to consider a systematic study of atomic total energies calculated with a self-consistent atomic structure code using the LDA parametrized by Perdew and Wang.[14] First, consider sp bonding materials. In Fig. 1 the error in calculating the energy to ''promote'' an electron from the s to p shell within the frozen core approximation minus that of the fully self-consistent result is plotted versus the number x of sp valence electrons in the 2nd, 3rd, and 4th rows of the Periodic Table. The error is less than 1 meV for elements in the 2nd row of the Periodic Table and less than 10 meV for most of the other elements. It decreases with increasing x, being larger for the alkali and alkaline-earth metals than for the halides. There is a jump in the error at $x \geqslant 3$ for Ga because of the completion of the $3d$ shell. This error can be essentially eliminated by including the $3d$ states as valence states in the self-consistent calculations. In Fig. 2 the error in calculating the energy to ''promote'' an electron from the s to d shell within the frozen core approximation minus that of the fully self-consistent result is plotted versus the number x of sd valence electrons in the 4th and 5th rows of the Periodic Table. Evidently, the frozen core error is considerably larger for sd materials than it is for

 © 1997 The American Physical Society

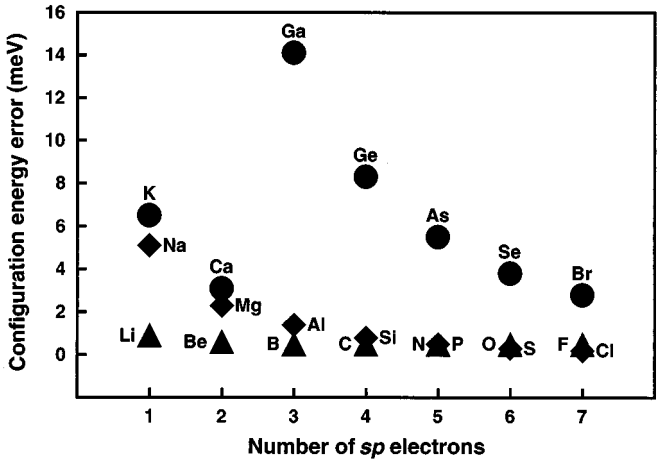

FIG. 1. Configuration energy error in meV corresponding to frozen core minus all-electron total energy differences $E(ns^{\sigma}np^{x-\sigma}\rightarrow ns^{\sigma-1}np^{x-\sigma+1})$, where x denotes the number of sp valence electrons in the neutral atom, σ is 1 for the alkali metal atoms and 2 otherwise, and n is the principal quantum number 2, 3, or 4.

sp materials, and is larger for the $3d$ transition metals than for the $4d$ transition metals. It is interesting that the error is uniformly positive (the promotion energy is larger in the frozen core approximation than in a fully relaxed calculation) even though the promotion energy itself changes sign for the sd materials at $x=6$. For all of these materials, the configuration energy error can be reduced by several orders of magnitude by including the upper core states in the self-consistent calculation.

Some examples of systems which have significant core-electron contributions to the structural energy have appeared in the literature. For example, Wright and Nelson[17] noted that it was necessary to include the $3d$ states to correctly calculate the structural properties of GaN and other Ga-containing materials. In our previous work,[18] we found that

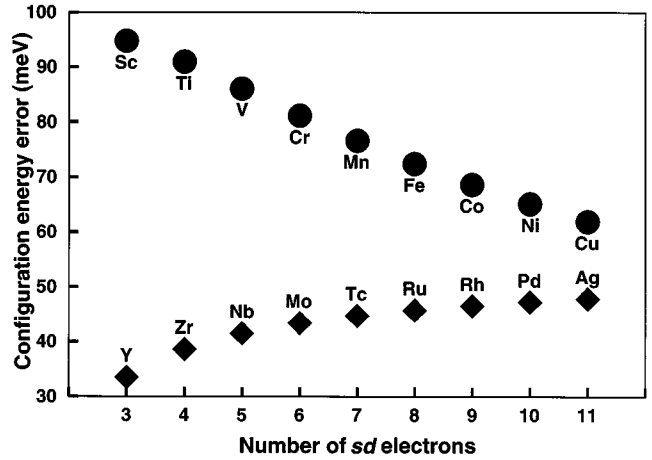

FIG. 2. Configuration energy error in meV corresponding to frozen core minus all-electron total energy differences $E[ns^2(n-1)d^{x-2}\rightarrow ns^1(n-1)d^{x-1}]$, where x denotes the number of sd valence electrons in the neutral atom and n denotes the principal quantum number 4 or 5.

pseudopotential calculations for FeS_2 determined the S-S bond length to be more than 0.1 Å larger than the experimental value, while all-electron calculations determined the bond length to be substantially closer to the experimental value. In the present paper, we find an even larger error in the pseudopotential prediction of the equilibrium lattice constant for CaF_2 compared with than that predicted by all-electron calculations. Clearly, it is sometimes necessary to go beyond the pseudopotential approach for structural simulations, as can be provided by the PAW formalism.

This paper is organized as follows. In Sec. II, we review the general features of formalism developed by Blöchl.[1] In Sec. III, we describe our method for constructing the basis and projector functions and present examples. In Sec. IV results are presented for calculation of the electronic structure of a variety of materials including the insulators CaF_2 and diamond; the semiconductors silicon and SiC; and the metals calcium and vanadium. The summary and conclusions are presented in Sec. V. Detailed formulas for the Hamiltonian matrix elements and total valence energy are presented in the Appendix.

II. GENERAL FORMALISM

In density functional theory[9] for periodic solids, it is necessary to calculate the self-consistent Bloch wave functions $\Psi_{n\mathbf{k}}(\mathbf{r})$, where n and $\mathbf{k}$ denote band index and wave vector, respectively. In the PAW formalism, all variational calculations are performed on smooth wave functions $\widetilde{\Psi}_{n\mathbf{k}}(\mathbf{r})$, which are designed to be represented in plane-wave expansions. The conversion between the smooth wave functions and the corresponding wave functions having the correct nodal form is achieved through the use of a set of three types of functions defined for each atom a: the ''all-electron'' (AE) basis functions $\phi_i^a(\mathbf{r})$,[19] the ''pseudo'' (PS) basis functions $\widetilde{\phi}_i^a(\mathbf{r})$, and the projector functions $\widetilde{p}_i^a(\mathbf{r})$. Blöchl[1] defined these functions to have the following properties. The AE and PS basis functions are chosen such that

$$\widetilde{\phi}_i^a(\mathbf{r})=\phi_i^a(\mathbf{r}) \quad \text{for} \quad r\geqslant r_c^a, \tag{1}$$

where r_c^a is the radius of a nonoverlapping sphere about the atomic site a. Because of the cancellation property (1), the basis functions ϕ_i^a and $\widetilde{\phi}_i^a$ are never evaluated beyond $r>r_c^a$, although they are continuous for all r. The projector functions vanish for $r>r_c^a$ and satisfy the complementary-orthogonality property:

$$\langle \widetilde{p}_i^a|\widetilde{\phi}_j^a\rangle=\delta_{ij}. \tag{2}$$

Within the constraints defined in Eqs. (1,2), there is considerable freedom in the choice of the atomic functions $\{\phi_i^a,\ \widetilde{\phi}_i^a,\ \text{and}\ \widetilde{p}_i^a\}$. The choices used in the present work will be described in Sec. III below. In terms of these functions, the full Bloch wave function $\Psi_{n\mathbf{k}}(\mathbf{r})$ can be calculated from the smooth wave function $\widetilde{\Psi}_{n\mathbf{k}}(\mathbf{r})$ using the relation

$$\Psi_{n\mathbf{k}}(\mathbf{r})=\widetilde{\Psi}_{n\mathbf{k}}(\mathbf{r})+\sum_{a,i}\ [\,\phi_i^a(\mathbf{r}-\mathbf{R}^a)-\widetilde{\phi}_i^a(\mathbf{r}-\mathbf{R}^a)]\langle\widetilde{p}_i^a|\widetilde{\Psi}_{n\mathbf{k}}\rangle, \tag{3}$$

where $\mathbf{R}^a$ denotes the atomic position within a unit cell.

The PAW formalism is designed so that the valence-electron density can be calculated as a sum of three contributions:

$$n(\mathbf{r}) = \tilde{n}(\mathbf{r}) + n^1(\mathbf{r}) - \tilde{n}^1(\mathbf{r}). \tag{4}$$

In Eq. (4), the first term represents the pseudodensity which can be represented by a plane-wave expansion throughout the unit cell. Specifically, the smooth density is given by

$$\tilde{n}(\mathbf{r}) \equiv \sum_{n\mathbf{k}} f_{n\mathbf{k}} |\tilde{\Psi}_{n\mathbf{k}}(\mathbf{r})|^2, \tag{5}$$

where $f_{n\mathbf{k}}$ denotes the occupancy factor. The last two contributions to Eq. (4) are designed to exactly cancel each other in the region outside the atomic spheres and to correct the density for the correct nodal behavior in the vicinity of each atom. The ''one-center'' terms can each be represented as a sum of atomic contributions $n^1(\mathbf{r}) \equiv \Sigma_a n^a(\mathbf{r}-\mathbf{R}^a)$ and $\tilde{n}^1(\mathbf{r}) \equiv \Sigma_a \tilde{n}^a(\mathbf{r}-\mathbf{R}^a)$. The atomic density terms are given by

$$n^a(\mathbf{r}) \equiv \sum_{n\mathbf{k},i,j} f_{n\mathbf{k}} \langle \tilde{\Psi}_{n\mathbf{k}} | \tilde{p}_i^a \rangle \langle \tilde{p}_j^a | \tilde{\Psi}_{n\mathbf{k}} \rangle \phi_i^a(\mathbf{r})^* \phi_j^a(\mathbf{r}), \tag{6}$$

for the contribution having the correct nodal form, and

$$\tilde{n}^a(\mathbf{r}) \equiv \sum_{n\mathbf{k},i,j} f_{n\mathbf{k}} \langle \tilde{\Psi}_{n\mathbf{k}} | \tilde{p}_i^a \rangle \langle \tilde{p}_j^a | \tilde{\Psi}_{n\mathbf{k}} \rangle \tilde{\phi}_i^a(\mathbf{r})^* \tilde{\phi}_j^a(\mathbf{r}), \tag{7}$$

for the corrections to $\tilde{n}$.

Blöchl derived the PAW formalism by writing the valence energy for the system in terms of three contributions corresponding to the density form:

$$E = \tilde{E} + E^1 - \tilde{E}^1. \tag{8}$$

The valence energy Eq. (8) represents the energy of the valence electrons interacting with themselves, with the atomic nuclei having atomic number Z^a, and with the core electrons of the system which are assumed to be ''frozen'' in the same functional form as in the atom.[20] The three contributions can be written as follows.

$\tilde{E}$ depends upon the evaluation of the smooth density functions throughout the unit cell:

$$\begin{aligned}\tilde{E} = &\sum_{n\mathbf{k}} f_{n\mathbf{k}} \left\langle \tilde{\Psi}_{n\mathbf{k}} \left| -\frac{\hbar^2}{2m}\nabla^2 \right| \tilde{\Psi}_{n\mathbf{k}} \right\rangle \\ &+ \frac{e^2}{2} \int\int d^3r\, d^3r' \frac{[\tilde{n}(\mathbf{r}) + \hat{n}(\mathbf{r})][\tilde{n}(\mathbf{r}') + \hat{n}(\mathbf{r}')]}{|\mathbf{r}-\mathbf{r}'|} \\ &+ e^2 \int\int d^3r\, d^3r' \frac{\tilde{n}(\mathbf{r})\tilde{n}_{\text{core}}(\mathbf{r}')}{|\mathbf{r}-\mathbf{r}'|} + \int d^3r\, \tilde{n}(\mathbf{r})\tilde{v}_{\text{loc}}(\mathbf{r}) \\ &+ \frac{e^2}{2} \int\int d^3r\, d^3r' \frac{\tilde{n}_{\text{core}}(\mathbf{r})\tilde{n}_{\text{core}}(\mathbf{r}')}{|\mathbf{r}-\mathbf{r}'|} + E_{\text{xc}}[\tilde{n} + \tilde{n}_{\text{core}}].\end{aligned} \tag{9}$$

The ''one-center'' contributions to Eq. (8) can each be represented as a sum of atomic terms $E^1 \equiv \Sigma_a E^a$ and $\tilde{E}^1 \equiv \Sigma_a \tilde{E}^a$, where a indexes all the atoms of the unit cell. Each one-center contribution, E^a and $\tilde{E}^a$, is evaluated with all integrals involved with evaluating the valence density contributions, confined within a sphere of radius r_c^a about the atom a. It can be shown that integrand of the difference energy $E^a - \tilde{E}^a$ converges smoothly to zero at the sphere boundary at r_c^a.

E^a represents the energy contribution inside the atomic sphere a:

$$\begin{aligned}E^a = &\sum_{n\mathbf{k},i,j} f_{n\mathbf{k}} \langle \tilde{\Psi}_{n\mathbf{k}} | \tilde{p}_i^a \rangle \langle \tilde{p}_j^a | \tilde{\Psi}_{n\mathbf{k}} \rangle \left\langle \phi_i^a \left| -\frac{\hbar^2}{2m}\nabla^2 \right| \phi_j^a \right\rangle \\ &+ \frac{e^2}{2} \int\int_{r,r' \le r_c^a} d^3r\, d^3r' \frac{n^a(\mathbf{r}) n^a(\mathbf{r}')}{|\mathbf{r}-\mathbf{r}'|} \\ &+ \int_{r \le r_c^a} d^3r\, n^a(\mathbf{r})[v_{\text{ion}}^a(r) + \tilde{v}_{\text{core}}(\mathbf{r})] \\ &+ E_{\text{xc}}[n^a + n_{\text{core}}^a - \tilde{n}_{\text{core}}^a + \tilde{n}_{\text{core}}] - E_{\text{xc}}[n_{\text{core}}^a].\end{aligned} \tag{10}$$

$\tilde{E}^a$ subtracts out the smooth density contributions included in Eq. (9) within atomic sphere a and includes additional Coulombic corrections terms:

$$\begin{aligned}\tilde{E}^a = &\sum_{n\mathbf{k},i,j} f_{n\mathbf{k}} \langle \tilde{\Psi}_{n\mathbf{k}} | \tilde{p}_i^a \rangle \langle \tilde{p}_j^a | \tilde{\Psi}_{n\mathbf{k}} \rangle \left\langle \tilde{\phi}_i^a \left| -\frac{\hbar^2}{2m}\nabla^2 \right| \tilde{\phi}_j^a \right\rangle \\ &+ \frac{e^2}{2} \int\int_{r,r' \le r_c^a} d^3r\, d^3r' \frac{\tilde{n}^a(\mathbf{r})\tilde{n}^a(\mathbf{r}')}{|\mathbf{r}-\mathbf{r}'|} \\ &+ \int_{r \le r_c^a} d^3r\, \tilde{n}^a(\mathbf{r})[\hat{v}^a(\mathbf{r}) + \tilde{v}_{\text{core}}(\mathbf{r})] \\ &+ \int_{r \le r_c^a} d^3r\, \tilde{n}^a(\mathbf{r})\tilde{v}_{\text{loc}}^a(\mathbf{r}) \\ &+ \hat{E}^a + \tilde{E}_{\text{core}}^a + \tilde{E}_{\text{core}}^{a0} + E_{\text{xc}}[\tilde{n}^a + \tilde{n}_{\text{core}}].\end{aligned} \tag{11}$$

In the above equations, E_{xc} denotes the exchange-correlation energy function which depends on the density argument.[10,21] In addition to depending on the valence density contributions (5, 6, and 7), the energy evaluation includes the frozen core density, a ''compensation'' charge density, and an arbitrary localized potential as discussed below.

The frozen core density $n_{\text{core}}^a(r)$ associated with site a is expected to be mostly contained within the atomic sphere r_c^a, however, because electrostatic effects are strong, a small extension of the core density beyond r_c^a can have an appreciable effect on the binding energy. We approximate these effects within the spirit of the frozen core approximation, by superposing the atomic core densities. For this purpose, it is convenient to define a spherically symmetric smooth core tail function associated with site a:

$$\tilde{n}_{\text{core}}^a(r) \equiv \begin{cases} \Gamma^a e^{-\gamma^a r^2}/4\pi & \text{for} \quad r \le r_c^a \\ n_{\text{core}}^a(r) & \text{for} \quad r \ge r_c^a \end{cases}, \tag{12}$$

where Γ^a and γ^a are adjustable constants. This form has been previously used for LAPW calculations.[22] In terms of the smooth core tail function, a smooth frozen core density function $\tilde{n}_{\text{core}}(\mathbf{r})$ can be formed from a lattice superposition, which can be easily evaluated in Fourier space:

$$\tilde{n}_{\rm core}(\mathbf{r}) = \frac{1}{\mathcal{V}} \sum_{\mathbf{G}} \bar{\tilde{n}}_{\rm core}(\mathbf{G}) e^{i\mathbf{G}\cdot\mathbf{r}},$$

where

$$\bar{\tilde{n}}_{\rm core}(\mathbf{G}) \equiv \sum_a e^{-i\mathbf{G}\cdot\mathbf{R}^a} \bar{\tilde{n}}^a_{\rm core}(G),$$

with

$$\bar{\tilde{n}}^a_{\rm core}(G) \equiv \int_0^\infty dr\ 4\pi r^2 \tilde{n}^a_{\rm core}(r) j_0(Gr), \tag{13}$$

where $\mathcal{V}$ is the volume of the unit cell, $\mathbf{R}^a$ denotes a lattice site, and $j_0(Gr)$ denotes the spherical Bessel function. The core tail potential which appears in Eqs. (10) and (11) is easily evaluated in Fourier space:

$$\tilde{v}_{\rm core}(\mathbf{r}) = \frac{4\pi e^2}{\mathcal{V}} \sum_{\mathbf{G}\neq 0} \frac{\bar{\tilde{n}}_{\rm core}(\mathbf{G})}{G^2} e^{i\mathbf{G}\cdot\mathbf{r}}, \tag{14}$$

where the $\mathbf{G}=0$ contribution must be treated separately as discussed below. The localized portion of the frozen core density contributes to Eq. (10) in the form of the ionic Coulomb potential for atom a (with atomic number Z^a):

$$v^a_{\rm ion}(r) \equiv e^2 \int_{r'\leqslant r^a_c} d^3r' \frac{n^a_{\rm ion}(r')}{|\mathbf{r}-\mathbf{r}'|},$$

where

$$n^a_{\rm ion}(r) \equiv -Z^a\ \delta(\mathbf{r}) + [n^a_{\rm core}(r) - \tilde{n}^a_{\rm core}(r)]. \tag{15}$$

Blöchl introduced a ''compensation'' charge density $\hat{n}^a$ in order to represent, in a physically correct and mathematically convenient form, the total charge within each atomic sphere a other than that represented by the smooth charge densities $\tilde{n}^a$ and $\tilde{n}^a_{\rm core}$ The total compensation charge density is given as the sum of atomic contributions $\hat{n}(\mathbf{r}) \equiv \Sigma_a \hat{n}^a(\mathbf{r}-\mathbf{R}^a)$ defined according to

$$\hat{n}^a(\mathbf{r}-\mathbf{R}^a) \equiv \sum_{LM} Q^a_{LM} Y_{LM}(\widehat{\mathbf{r}-\mathbf{R}^a}) g^a_L(|\mathbf{r}-\mathbf{R}^a|). \tag{16}$$

In Eq. (16), the coefficients Q^a_{LM} represent the multipole moments of the compensation charge:

$$Q^a_{LM} \equiv (-Z^a + Q^a_{\rm core})\,\delta_{L0}\delta_{M0} + \sqrt{4\pi}\int_{(r\leqslant r^a_c)} d^3r\ Y^*_{LM}(\hat{\mathbf{r}}) r^L [n^a(\mathbf{r}) - \tilde{n}^a(\mathbf{r})], \tag{17}$$

where $Q^a_{\rm core}$ is the core charge localized within the atomic sphere,

$$Q^a_{\rm core} \equiv \int_{r\leqslant r^a_c} d^3r\ [n^a_{\rm core}(r) - \tilde{n}^a_{\rm core}(r)], \tag{18}$$

and where the integrals in Eqs. (17) and (18) are taken over a sphere of radius r^a_c centered at atom a. Since the compensation charge is used to represent the correct Coulombic potential outside the atomic spheres, its functional form inside the spheres is arbitrary. It is convenient to choose a normalized form based on a Gaussian times r^L:

$$g^a_L(r) \equiv \mathcal{N}_L r^L e^{-r^2/\sigma_a^2},$$

where

$$\mathcal{N}_L \equiv \left[\sqrt{4\pi}\int_0^\infty dr\ r^{2(L+1)} e^{-r^2/\sigma_a^2}\right]^{-1}. \tag{19}$$

Here σ_a is a width parameter adjusted so that $g^a_L(r)\approx 0$ for $r\geqslant r^a_c$. In Eq. (11), $\hat{v}^a$ denotes the Coulomb potential of the compensation charge density $\hat{n}^a$, and $\hat{E}^a$ denotes the corresponding self-energy correction:

$$\hat{v}^a(\mathbf{r}) \equiv e^2 \int d^3r' \frac{\hat{n}^a(\mathbf{r}')}{|\mathbf{r}-\mathbf{r}'|} \quad \text{and}$$

$$\hat{E}^a \equiv \frac{e^2}{2}\int d^3r\ d^3r' \frac{\hat{n}^a(\mathbf{r})\hat{n}^a(\mathbf{r}')}{|\mathbf{r}-\mathbf{r}'|}. \tag{20}$$

Additional Coulombic correction terms appear in Eq. (11). The term $\tilde{E}^a_{\rm core}$ represents ion-core interactions minus the corresponding self-energy corrections:

$$-\tilde{E}^a_{\rm core} \equiv \int d^3r\ n^a_{\rm ion}(|\mathbf{r}-\mathbf{R}^a|)[\tilde{v}_{\rm core}(\mathbf{r}) - \tilde{v}^a_{\rm core}(|\mathbf{r}-\mathbf{R}^a|)] - \frac{e^2}{2}\int\int d^3r\ d^3r' \frac{\tilde{n}^a_{\rm core}(r)\tilde{n}^a_{\rm core}(r')}{|\mathbf{r}-\mathbf{r}'|}. \tag{21}$$

In this expression $\tilde{v}_{\rm core}$ (14) represents the potential due to the superposed core densities, while the $\tilde{v}^a_{\rm core}$ term subtracts out the potential due to the smooth core density function $\tilde{n}^a_{\rm core}$ associated with the site a. By subtracting out self-Coulomb interactions, the net ionic contributions of this calculation are equivalent to that evaluated via an Ewald[23] summation in other formulations.[24]

Because the analysis represents a system with no net charge, the Coulomb energy is well defined. However, special care is needed for evaluating the $\mathbf{G}=\mathbf{0}$ contributions. The compensation charge (16) has been defined so that the sum of the smooth charge density plus the core tail density plus the compensation charge density represent a neutral system: $\int d^3r[\tilde{n}(\mathbf{r}) + \tilde{n}_{\rm core}(\mathbf{r}) + \hat{n}(\mathbf{r})] = 0$. Also by construction (16), the sum of ionic charges plus valence difference charge minus the compensation charge also form a neutral system: $\int d^3r[n^a_{\rm ion}(r) + n^a(\mathbf{r}) - \tilde{n}^a(\mathbf{r}) - \hat{n}^a(\mathbf{r})] = 0$. However, in collecting all the terms involved with evaluating the Coulomb interaction in reciprocal space, one finds a nonvanishing contribution of the form

$$-\tilde{E}^{a0}_{\rm core} \equiv \frac{4\pi e^2 \tilde{n}_{\rm core}(0)}{\mathcal{V}} \lim_{\mathbf{G}\to 0}\left[\frac{[\overline{n^a_{\rm ion}}(\mathbf{G}) + \overline{n^a}(\mathbf{G}) - \bar{\tilde{n}}^a(\mathbf{G}) - \overline{\hat{n}^a}(\mathbf{G})]}{G^2}\right]. \tag{22}$$

The energy expressions of Eqs. (9), (11) include an extra potential term introduced in the original formulation of Blöchl[1] of the form $\tilde{v}_{\rm loc}(\mathbf{r}) \equiv \Sigma_a \tilde{v}^a_{\rm loc}(\mathbf{r}-\mathbf{R}^a)$, where $\tilde{v}^a_{\rm loc}$ is an arbitrary potential localized within the r^a_c radius of atom a.

This localized potential introduces no net contribution to the energy and in the present work was set identically to zero.

The self-consistent Schrödinger equations were obtained by Blöchl[1] by applying the variational principle for the smooth wave functions $\tilde{\Psi}_{n\mathbf{k}}(\mathbf{r})$ to minimize the valence energy (8) subject to the appropriate orthonormality constraints. The resulting equations take the form of a generalized eigenvalue problem:

$$\tilde{H}\,\tilde{\Psi}_{n\mathbf{k}}(\mathbf{r})=\varepsilon_{n\mathbf{k}}\tilde{O}\,\tilde{\Psi}_{n\mathbf{k}}(\mathbf{r}). \tag{23}$$

The effective Hamiltonian operator can be expressed in the form

$$\tilde{H}\equiv\tilde{H}^{\mathrm{PW}}+\sum_{a,(i,j)}|\tilde{p}_i^a\rangle D_{ij}^a\langle\tilde{p}_j^a|. \tag{24}$$

The first term has the form of a local pseudopotential Hamiltonian:

$$\tilde{H}^{\mathrm{PW}}\equiv-\frac{\hbar^2}{2m}\nabla^2+\tilde{v}_{\mathrm{eff}}(\mathbf{r}), \tag{25}$$

where the smooth effective potential is given by

$$\tilde{v}_{\mathrm{eff}}(\mathbf{r})\equiv e^2\int d^3r'\,\frac{[\tilde{n}(\mathbf{r}')+\tilde{n}_{\mathrm{core}}(\mathbf{r}')+\hat{n}(\mathbf{r}')]}{|\mathbf{r}-\mathbf{r}'|}+\tilde{v}_{\mathrm{loc}}(\mathbf{r})+\mu_{\mathrm{xc}}[\tilde{n}(\mathbf{r})+\tilde{n}_{\mathrm{core}}(\mathbf{r})], \tag{26}$$

where μ_{xc} represents the exchange-correlation potential.[10] The orthonormality matrix in Eq. (23) is given by

$$\tilde{O}\equiv\mathbb{1}+\sum_{a,(i,j)}|\tilde{p}_i^a\rangle O_{ij}^a\langle\tilde{p}_j^a|,$$

where

$$O_{ij}^a\equiv\langle\phi_i|\phi_j\rangle-\langle\tilde{\phi}_i|\tilde{\phi}_j\rangle. \tag{27}$$

The one-center contributions to the effective Hamiltonian (24) are functionally similar to nonlocal pseudopotential terms. For each atom, they can be expressed in terms of AE or PS matrix elements:

$$D_{ij}^a=H_{ij}^a-\tilde{H}_{ij}^a,$$

where,

$$H_{ij}^a\equiv\langle\phi_i^a|H^a|\phi_j^a\rangle$$

and

$$\tilde{H}_{ij}^a\equiv\langle\tilde{\phi}_i^a|\tilde{H}^a|\tilde{\phi}_j^a\rangle. \tag{28}$$

These terms are discussed in more detail in the Appendix. In the present work, studying systems with fixed atomic positions $\{\mathbf{R}^a\}$, self-consistent solutions to Eq. (23) were obtained with a combination of direct diagonalization using a combination of the Davidson-Liu algorithm[25] and conjugate gradient[12] techniques.

III. PAW BASIS AND PROJECTOR FUNCTIONS

A. Formalism

The PAW method depends upon finding basis and projector functions. There have been several suggestions by Blöchl[1] and his collaborators[4] for constructing the basis and projector functions. The procedure that we have found to work well is similar to that developed by Vanderbilt[2] in his soft pseudopotential technique and is also similar to ''generalized separable potentials'' developed in an earlier work of Blöchl.[3]

The starting point of the construction is the solution of the all-electron self-consistent Schrödinger equation for the atom.[26,27] Since the atom has spherical symmetry, the interesting part of a AE basis function is its radial function $\phi_{n_il_i}^a(r)$, although the complete set of basis functions is composed of products of the radial function and the appropriate spherical harmonic functions: $\phi_i^a(\mathbf{r})\equiv(\phi_{n_il_i}^a(r)/r)Y_{l_im_i}(\hat{\mathbf{r}})$.[19] In general, the radial AE basis functions $\{\phi_{n_il_i}^a(r)\}$ are chosen as the valence eigenstates of the AE Schrödinger equation; their corresponding energies are denoted by $\{\varepsilon_{n_il_i}^a\}$. For atoms with upper core states which are involved in the bonding, it is necessary to include these states among the basis functions. In some cases, it may also be necessary to include some unbound states among the basis functions. For simplicity in notation, the index n_i is used to denote the principal quantum number for bound states and is extended to enumerate any continuum states included in the basis set. All evaluations with these functions are confined to the region $r\leqslant r_c^a$. For each l value, at most two radial basis functions were needed for all of the systems we have studied so far.

For each radial AE basis function $\phi_{n_il_i}^a(r)$, the corresponding radial PS basis function is chosen to have a polynomial form

$$\tilde{\phi}_{n_il_i}^a(r)=r^{l_i+1}\sum_{\nu=0}^{N-1}a_\nu r^{2\nu}, \tag{29}$$

where N is an even number between 4 and 10, and where the coefficients a_ν are determined from the following two matching sets of conditions:

$$\tilde{\phi}_{n_il_i}^a(r_k)=\phi_{n_il_i}^a(r_k), \tag{30}$$

and

$$-\frac{\hbar^2}{2m}\left(\frac{d^2}{dr_k^2}-\frac{l_i(l_i+1)}{r_k^2}\right)\tilde{\phi}_{n_il_i}^a(r_k)=[\varepsilon_{n_il_i}^a-v_{\mathrm{eff}}^a(r_k)]\phi_{n_il_i}^a(r_k), \tag{31}$$

where $v_{\mathrm{eff}}^a(r)$ is the all-electron self-consistent effective potential for the spherically symmetric atom, which is given by

$$v_{\mathrm{eff}}^a(r)\equiv-\frac{e^2Z^a}{r}+e^2\int d^3r'\,\frac{[n^a(r')+n_{\mathrm{core}}^a(r')]}{|\mathbf{r}-\mathbf{r}'|}+\mu_{\mathrm{xc}}[n^a(r)+n_{\mathrm{core}}^a(r)]. \tag{32}$$

The N equations corresponding to Eqs. (30) and (31), expressed in terms of the polynomial expansion (29), are solved simultaneously at $N/2$ consecutive numerical mesh points $\{r_k\}$, where $k_0 \leq k < k_0 + N/2$, and $r_{k_0} \leq r_c^a$ to determine the N coefficients $\{a_\nu\}$. The first set of equations (30) ensures that the cancellation condition (1) is satisfied for the first $(N-1)/2$ derivatives of the PS basis function, while the second set of equations (31) ensures that the projector functions are well behaved.

Using the radial PS basis functions (29), we can construct the radial projector functions using the same functions developed by Vanderbilt[2] for his soft nonlocal pseudopotential which are also very similar to Blöchl's ''generalized separable potentials.''[3] For each atom a and angular momentum l, the matrix elements of the PS basis functions can be defined:

$$B^{al}_{nn'} \equiv \int_0^{r_c^a} dr\ \widetilde{\phi}^a_{nl}(r) \left[-\frac{\hbar^2}{2m}\left(\frac{d^2}{dr^2} - \frac{l(l+1)}{r^2}\right) + \widetilde{v}^a_{\rm eff}(r) - \varepsilon^a_{n'l} \right] \widetilde{\phi}^a_{n'l}(r), \tag{33}$$

where $\widetilde{v}^a_{\rm eff}(r)$ is the atomic PS effective potential given by

$$\widetilde{v}^a_{\rm eff}(r) \equiv \hat{v}^a(r) + e^2 \int d^3r' \frac{[\widetilde{n}^a(r') + \widetilde{n}^a_{\rm core}(r')]}{|\mathbf{r}-\mathbf{r}'|} + \widetilde{v}^a_{\rm loc}(r) + \mu_{\rm xc}[\widetilde{n}^a(r) + \widetilde{n}^a_{\rm core}(r)], \tag{34}$$

where the potential due to the ''compensation'' charge of the atom is given by $\hat{v}^a(r) = e^2\ Q^a_{00}\ {\rm erf}(r/\sigma_a)/r$. In the present work, we have set the arbitrary localized potential $\widetilde{v}^a_{loc}(r)$ identically equal to zero. Since, by construction, $v^a_{\rm eff}(r) \equiv \widetilde{v}^a_{\rm eff}(r)$ for $r \geq r_c^a$, the integrand in Eq. (33) vanishes as $r \to r_c^a$. The radial projector functions can be defined:

$$\widetilde{p}^a_{nl}(r) \equiv \sum_{n'} \left[-\frac{\hbar^2}{2m}\left(\frac{d^2}{dr^2} - \frac{l(l+1)}{r^2}\right) + \widetilde{v}^a_{\rm eff}(r) - \varepsilon^a_{n'l} \right] \widetilde{\phi}^a_{n'l}(r)\ (\mathbf{B}^{al})^{-1}_{n'n}. \tag{35}$$

For the same reason that the argument of Eq. (33) vanishes as $r \to r_c^a$, the radial projector function, $\widetilde{p}^a_{nl}(r)$, also vanishes for $r > r_c^a$. The radial projector functions calculated from Eq. (35) are related to the full projector functions according to $\widetilde{p}^a_i(\mathbf{r}) \equiv (\widetilde{p}^a_{n_i l_i}(r)/r) Y_{l_i m_i}(\hat{\mathbf{r}})$. This construction of the projector functions is very similar to the ''local wave function'' $|\beta_i\rangle$ defined by Vanderbilt.[2] With this choice, the second term of the effective Hamiltonian (24) is essentially the same as the nonlocal potential operator defined by Vanderbilt.[2] Provided that $\hat{n}^a(\mathbf{r}) \equiv 0$ for $r \geq r_c^a$, the projector function (35) vanishes for $r \geq r_c^a$ and satisfies the quasiorthonormality condition (2). It is constructed so that the PS basis functions $\{\widetilde{\phi}^a_i(\mathbf{r})\}$ are exact solutions to the PAW Schrödinger Eq. (23). This formulation of the projector functions is consistent with the guidelines developed by Blöchl.

With the above scheme for constructing the atomic functions, the accuracy and convergence of the calculation is controlled by the following considerations.

(a) The set of the radial AE basis functions $\{\phi^a_{n_i l_i}\}$ should be chosen to completely represent the valence wave functions within the atomic spheres. As discussed below, it is sometimes necessary to augment this set of functions with the upper core functions and some continuum functions for higher angular momentum components.

(b)The atomic radii r_c^a should be chosen to be as large as possible to facilitate the convergence of the smooth functions in Fourier space, but there must be no overlap of atomic spheres for all structures to be studied.

(c) The shape of each PS basis functions $\{\widetilde{\phi}^a_{n_i l_i}\}$ and the corresponding projector function $\{\widetilde{p}^a_{n_i l_i}\}$ can be controlled by adjusting the matching point r_{k_0} and the number N of matching coefficients $\{a_\nu\}$ used to satisfy equations (30) and (31). In general the best numerical properties are obtained by ensuring that for a given angular momentum component l_i, the first projector function $\{\widetilde{p}^a_{n_i l_i}\}$ has no nodes, the second has one node, etc., since the projector functions take the role of an approximate orthogonal function expansion.

It is convenient to choose one value of the atomic radius r_c^a for each atom, while the parameters r_{k_0} and N can be different for each radial AE function $\phi^a_{n_i l_i}$. Although the shapes of the functions are sensitive to the choice of these parameters, the total energy is not sensitive.

B. Example functions

Blöchl[1,3] showed and we have verified that it is generally possible to perform accurate calculations with a minimal basis including one set of PAW functions for each $n_i l_i$ upper core and valence orbital. In addition, it is sometimes important to augment this ''minimal'' basis with some continuum states. For example, for Si, it was necessary to include a continuum $l=2$ function which we denote ϵd. In Table I are listed some representative PAW basis parameters and their corresponding configuration energy errors. From this table, it is apparent that for atomic calculations, this procedure makes it possible to achieve an accuracy close to the accuracy of the frozen core approximation itself. With the exception of the valence-only basis set of V, all of these functions correspond to a configuration energy error of less than a few meV. For the valence-only basis set of V, the configuration energy error is less than $\frac{1}{4}$th of the error in the frozen core approximation.

Plots of the PAW functions are shown for V in Figs. 3 and 4, comparing the set including the valence functions $\{4s,\ 4p,\ 3d\}$ only and the more complete set including the upper core and valence functions $\{3s,\ 4s,\ 3p,\ 4p,\ 3d\}$, respectively. These functions were constructed using the parameters listed in Table I. The shapes of these functions are representative of those of the other atoms listed in Table I.

From the atomic analysis of the accuracy of the configuration energies, as well as the accuracy of the energy eigenvalues and logarithmic derivatives, we expect that the set including the upper core states (Fig. 4) will give more accurate results than the valence only set (Fig. 3). In fact, the valence-only set was found to suffer from ''ghost'' states[28,29] and therefore yielded no meaningful results.

TABLE I. List of PAW basis function parameters for atoms in this study. Radial parameters r_c^a and r_{k_0} are given in bohr units. Errors in the sp or sd ''promotion'' energies (as defined in the figure captions of Figs. 1 and 2) are listed in order to indicate the accuracy of the calculations. ΔE_{PAW} (in meV units) indicates the magnitude of the difference between the ''promotion'' energy calculated using the PAW formalism relative to that of a frozen core calculation. $\Delta E_{\mathrm{relax}}$ (in meV units) indicates the magnitude of the difference between the ''promotion'' energy calculated using the frozen core approximation relative to that of the fully relaxed result.

Atom (Z)	r_c^a	{Basis functions (r_{k_0})}	ΔE_{PAW}	$\Delta E_{\mathrm{relax}}$	Ghost states ?
C (6)	1.2	$\{2s(1.2),2p(0.85)\}$	0.04	0.46	no
F (9)	1.2	$\{2s(1.2),2p(0.8)\}$	2.04	0.47	no
Si (14)	2.2	$\{3s(2.2),3p(2.0),\epsilon d(1.4)\}$	0.95	0.78	no
Ca (20)	3.6	$\{4s(3.6),4p(3.6),3d(2.0)\}$	0.88	3.06	yes
Ca (20)	2.7	$\{3s(2.7),4s(2.7),3p(2.7),4p(2.7),3d(1.5)\}$	0.06	0.00	no
V (23)	2.3	$\{4s(2.3),4p(2.3),3d(1.25)\}$	17.05	85.99	yes
V (23)	2.1	$\{3s(2.1),4s(2.1),3p(2.1),4p(2.1),3d(1.0)\}$	3.01	0.28	no

The problem of ghost states for separable nonlocal pseudopotentials has been well documented in the literature.[8,28,29] Since the PAW Hamiltonian has the same mathematical form, it is also subject to this problem. Table I indicates which of the PAW function sets are found to have caused ghost states in solid state calculations involving that atom. For both Ca and V, we investigated a range of PAW parameters in an unsuccessful attempt to generate ghost-free valence-only basis sets. However, for each of these materials the more complete basis set, which included the upper core states, was not only ghost free but also more accurate according to the atomic criteria.

However, since the ghost problem has been identified in this formulation of the PAW formalism, one is motivated to find ways of improving the PAW basis function construction algorithm. One possibility might be that a convenient form for the localized potential functions $\tilde{v}_{\mathrm{loc}}^a(r)$ could reduce the ghost problem. This will be considered in future work.

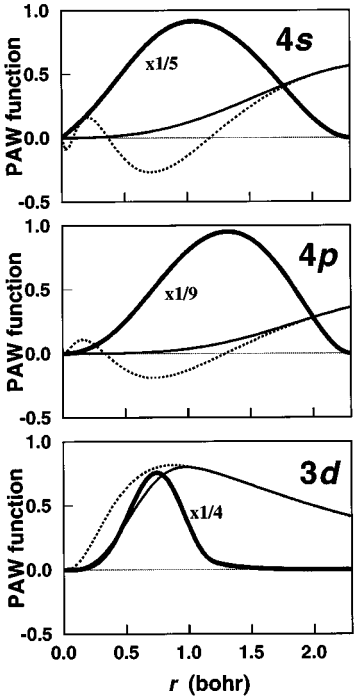

FIG. 3. Vanadium PAW functions for a minimal basis set (valence only), including $4s$, $4p$, and $3d$ functions; with the dashed line indicating $\phi_{n_i l_i}(r)$, the thin solid line indicating $\tilde{\phi}_{n_i l_i}(r)$, and a thick solid line indicating a scaled plot of $\tilde{p}_{n_i l_i}(r)$. This set of functions was constructed using the calculational parameters listed in Table I, and has ghost state difficulties.

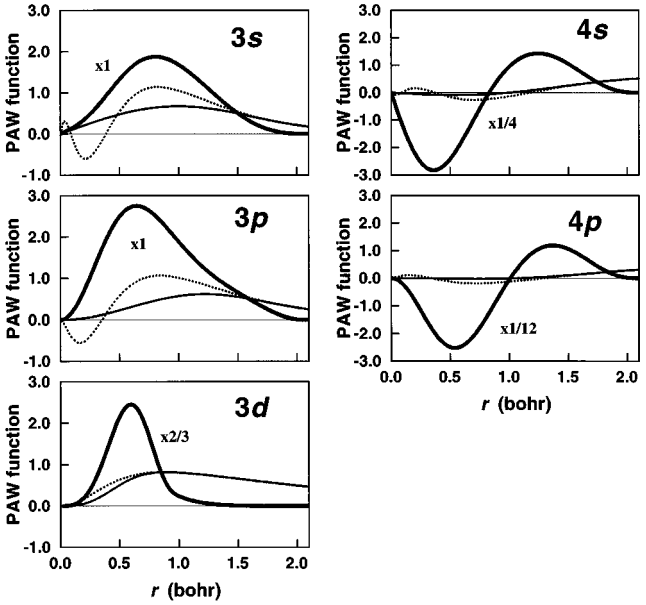

FIG. 4. Vanadium PAW functions for an accurate basis set (including upper core states), including $3s$, $4s$, $3p$, $4p$, and $3d$ functions; with the dashed line indicating $\phi_{n_i l_i}(r)$, the thin solid line indicating $\tilde{\phi}_{n_i l_i}(r)$, and the thick solid line indicating a scaled plot of $\tilde{p}_{n_i l_i}(r)$. This set of functions was constructed using the calculational parameters listed in Table I, and has no ghost state difficulties.

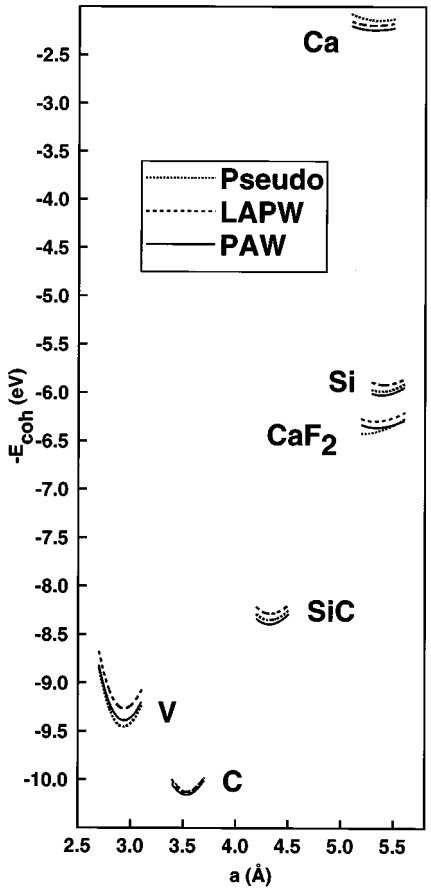

FIG. 5. Plot of the negative of the cohesive energy per atom (in eV) versus lattice constant (in Å) for all of the materials in this study, comparing results obtained using pseudopotential, LAPW, and PAW codes. Results include V (bcc structure), C and Si (diamond structure), SiC (zinc blende structure), Ca (fcc structure), and CaF_2 (fluorite stucture).

IV. RESULTS FOR SOME REPRESENTATIVE COVALENT AND IONIC MATERIALS

In order to check the accuracy of the PAW formalism for bulk materials, we have carried out a series of density-functional calculations, comparing results obtained using the PAW code with that obtained using LAPW (Ref. 8) and mixed-basis pseudopotential[7,13] codes. The PAW calculations were performed using the larger basis sets described in Table I. Care was taken to ensure that all the calculations were equivalently converged. All Brillouin zone integrals were performed using a uniform sampling of k points with a Gaussian weighting scheme.[30] Results for the calculated cohesive energies versus lattice constant are plotted in Fig. 5, showing results for diamond, silicon, SiC, and CaF_2, fcc Ca, and bcc V. These results were fit to Murnaghan's equation[31] to obtain values of the cohesive energy, lattice constant, and bulk modulus summarized in Table II. In calculating the cohesive energies, no corrections were made for atomic multiplet energies, or zero point motion. As expected,[15] the LDA results predict a smaller lattice constant and larger cohesive energies and bulk moduli than the experimental values. While focus of the present study is on the comparison of the three calculation schemes to each other, it is gratifying to note that the present results are also consistent with previous calculations.[34–36] Uniform shifts of the cohesive energies are due to small sensitivies of the three methods to their calculational parameters such as muffin-tin or atomic sphere radii, plane-wave cutoff's, or partial-wave convergence. However, with the exception of CaF_2, the three methods give nearly identically shaped plots of cohesive energy $(-E_{\mathrm{coh}})$ versus lattice constant (a), as shown in Fig. 5, and very close values for the equilibrium lattice constants (within 1%) and bulk moduli (within 5%), as shown in Table II.

For CaF_2, the pseudopotential calculation predicts a lattice constant which is 2% (more than 0.1 Å) smaller and a bulk modulus which is $10-20$ % smaller than the PAW and LAPW results. Since the pseudopotential calculation is a va-

TABLE II. Comparison of cohesive energies, E_{coh} (eV/atom); equilibrium lattice constants, a_0 (Å); and bulk moduli, B (GPa) calculated using the PAW, LAPW, and pseudopotential formalisms.

		E_{coh}	a_0	B
Diamond	PAW	10.16	3.54	460
	LAPW	10.13	3.54	470
	pseudopotential	10.13	3.54	460
	experiment	7.37[a]	3.56[a]	443[a]
Silicon	PAW	6.03	5.38	98
	LAPW	5.92	5.41	98
	pseudopotential	5.99	5.39	98
	experiment	4.63[a]	5.43[a]	99[a]
SiC	PAW	8.39	4.32	220
	LAPW	8.29	4.33	230
	pseudopotential	8.35	4.33	230
	experiment	6.34[b]	4.36[b]	224[b]
CaF_2	PAW	6.36	5.34	100
	LAPW	6.30	5.33	110
	pseudopotential	6.42	5.21	90
	experiment	5.36[c]	5.445[c]	85-90[c]
fcc Ca	PAW	2.24	5.32	19
	LAPW	2.20	5.33	19
	pseudopotential	2.14	5.37	20
	experiment	1.84[a]	5.58[a]	15[a]
bcc V	PAW	9.39	2.94	200
	LAPW	9.27	2.94	200
	pseudopotential	9.46	2.94	210
	experiment	5.31[a]	3.03[a]	162[a]

[a]Reference 32.
[b]Reference 34.
[c]Reference 33.

lence only calculation, while both the PAW and LAPW calculations include the relaxation of the upper core electrons, we can conclude that core effects are important for describing the structural properties of this system. This conclusion is consistent with the configuration energy errors discussed in Sec. I. An additional contributing factor for this system is the fact that the valence levels of F (especially the $2s$ state) are energetically close to the upper core levels ($3s$ and $3p$ states) of Ca.

One might have expected core relaxation effects to be important in more of the systems that we have studied. For fcc Ca, the structural errors of the valence-only (pseudopotential) calculation are much smaller than that of CaF_2. Figure 2 would lead one to expect a large core relaxation effect for bcc V, but as shown in Fig. 5, this is not the case. We would also have expected KF to have appreciable core relaxation effects. However, preliminary results indicate that core relaxation effects are much less important for KF than for CaF_2.

V. SUMMARY AND CONCLUSIONS

In summary, we have successfully implemented a version of the PAW method for electronic structure calculations. We have calculated the cohesive energy as a function of lattice constant for six representative crystals—diamond, silicon, SiC, CaF_2, fcc Ca, and bcc V. The results are consistent with results obtained with the well-established LAPW and pseudopotential electronic structure methods. For diamond, silicon, SiC, fcc Ca, and bcc V the PAW results were essentially the same as the LAPW and pseudopotential results. For CaF_2, there is an indication that the PAW approach is able to represent the cohesive properties more accurately than can the pseudopotential approach by including the contributions from the upper core states of Ca. Further work is needed to fine tune the construction algorithm for the PAW basis and projector functions in order to avoid the problem of ghost states.[28,29]

The present implementation is not yet optimized for efficiency, and is similar in computation effort to the pseudopotential approach. The results are encouraging for both the inherent accuracy and efficiency of the PAW algorithm, making it a very attractive method first-principles dynamical calculations.[4–6]

ACKNOWLEDGMENTS

The computations for this project were supported by NSF Grant No. DMR-9403009. We would also like to thank Peter Blöchl for helpful information during the early stages of this project. We would also like to thank Peter Blaha for helping us use the WIEN95 code.

APPENDIX: HAMILTONIAN MATRIX ELEMENTS

In using the PAW method for periodic systems, the smooth wave function $\widetilde{\Psi}_{n\mathbf{k}}(\mathbf{r})$ are conveniently represented in terms of a plane-wave expansion:

$$\widetilde{\Psi}_{n\mathbf{k}}(\mathbf{r}) = \sqrt{\frac{1}{\mathcal{V}}}\sum_{\mathbf{G}} A_{n\mathbf{k}}(\mathbf{G}) e^{i(\mathbf{k}+\mathbf{G})\cdot\mathbf{r}}, \tag{A1}$$

where $\mathcal{V}$ denotes the volume of the unit cell. The plane-wave expansion coefficients $A_{n\mathbf{k}}(\mathbf{G})$ are then the variational parameters of the problem which are determined by evaluating Eq. (23) in a plane-wave representation. The $\widetilde{H}^{\mathrm{PW}}$ contribution of the PAW Hamiltonian (25) can easily then be evaluated in Fourier space using a formalism similar to that developed for pseudopotentials.[24] The Fourier transform of the smooth density (5) can be represented by

$$\bar{\tilde{n}}(\mathbf{G}) \equiv \int_{\mathcal{V}} d^3r\ \tilde{n}(\mathbf{r}) e^{-i\mathbf{G}\cdot\mathbf{r}}. \tag{A2}$$

The Fourier transform of the compensation charge (16) density takes the form

$$\overline{\hat{n}}(\mathbf{G}) = \sum_{a,LM} Q^a_{LM} Y_{LM}(\hat{\mathbf{G}}) e^{-i\mathbf{G}\cdot\mathbf{R^a}}\ \overline{g^a_L}(G), \tag{A3}$$

where

$$\overline{g^a_L}(G) = \frac{\sqrt{4\pi}\ i^{-L}}{(2L+1)!!}\ G^L e^{-G^2\ \sigma_a^2/4}. \tag{A4}$$

The Fourier transform of the core tail density has been defined in Eq. (13). The Fourier transform of the arbitrary localized potential function can be represented by

$$\bar{\tilde{v}}_{\mathrm{loc}}(\mathbf{G}) = \sum_a\ e^{-i\mathbf{G}\cdot\mathbf{R^a}}\ \bar{\tilde{v}}^a_{\mathrm{loc}}(G),$$

where

$$\bar{\tilde{v}}^a_{\mathrm{loc}}(G) \equiv \int_0^\infty dr\ 4\pi r^2 \tilde{v}^a_{\mathrm{loc}}(r) j_0(Gr). \tag{A5}$$

In these terms, the smooth energy contribution (9) can be evaluated using the same techniques as used in the pseudopotential formalism:[24]

$$\begin{aligned}\widetilde{E} = {} & \frac{\hbar^2}{2m}\sum_{n\mathbf{k}} f_{n\mathbf{k}}\left(\sum_{\mathbf{G}} |A_{n\mathbf{k}}(\mathbf{G})|^2\ \ |\mathbf{k}+\mathbf{G}|^2\right) \\ & + \frac{2\pi e^2}{\mathcal{V}}\sum_{\mathbf{G}\neq 0} \frac{|\bar{\tilde{n}}(\mathbf{G})+\bar{\tilde{n}}(\mathbf{G})|^2 + |\bar{\tilde{n}}_{\mathrm{core}}(\mathbf{G})|^2}{G^2} \\ & + \frac{4\pi e^2}{\mathcal{V}}\sum_{\mathbf{G}\neq 0} \frac{\bar{\tilde{n}}^*(\mathbf{G})\bar{\tilde{n}}_{\mathrm{core}}(\mathbf{G})}{G^2} \\ & + \frac{1}{\mathcal{V}}\sum_{\mathbf{G}}\ \bar{\tilde{n}}^*(\mathbf{G})\bar{\tilde{v}}_{\mathrm{loc}}(\mathbf{G}) \\ & + \int_{\mathcal{V}} d^3r[\tilde{n}(\mathbf{r})+\tilde{n}_{\mathrm{core}}(\mathbf{r})]\epsilon_{\mathrm{xc}}[\tilde{n}(\mathbf{r})+\tilde{n}_{\mathrm{core}}(\mathbf{r})],\end{aligned} \tag{A6}$$

where the last term (the exchange-correlation contribution) is evaluated by trapezoidal rule integration using the real space fast Fourier transform grid.[7] The corresponding Hamiltonian function $\widetilde{H}^{\mathrm{PW}}$ (25) can be written

$$\tilde{H}^{\mathrm{PW}} = -\frac{\hbar^2}{2m}\nabla^2 + \frac{4\pi e^2}{\mathcal{V}}\sum_{\mathbf{G}\neq 0}\frac{[\bar{\tilde{n}}(\mathbf{G})+\overline{\tilde{n}(\mathbf{G})}+\bar{\tilde{n}}_{\mathrm{core}}(\mathbf{G})]}{G^2}e^{i\mathbf{G}\cdot\mathbf{r}} + \frac{1}{\mathcal{V}}\sum_{\mathbf{G}}\bar{\tilde{v}}_{\mathrm{loc}}(\mathbf{G})\ e^{i\mathbf{G}\cdot\mathbf{r}} + \mu_{\mathrm{xc}}[\tilde{n}(\mathbf{r})+\tilde{n}_{\mathrm{core}}(\mathbf{r})]. \tag{A7}$$

The contributions to the PAW Hamiltonian (23) from the atomic basis and projector functions need some additional consideration. In general, it is convenient to make use of atomic parameters calculated and stored during the process of constructing the basis and projector functions for each atom.

The scalar constants that need to be stored for each atom are Z^a, the atomic number; Q^a_{core}, the frozen core charge; r^a_c, the PAW matching radius; σ_a, the compensation charge width parameter; and Γ^a and γ^a, the core tail function parameters. The radial functions that need to be stored on radial grid for each atom are $n^a_{\mathrm{core}}(r)$, the core density; $\{\phi^a_{n_i l_i}\}$, the atomic AE basis functions; $\{\tilde{\phi}^a_{n_i l_i}\}$, the corresponding PS basis functions; and $\{\tilde{p}^a_{n_i l_i}\}$, the corresponding projector functions.

The ''one-center'' radial integrals that are needed in the evaluation of the overlap and Hamiltonian matrix elements, O^a_{ij} [Eq. (27)] and D^a_{ij} [Eq. (28)], are conveniently calculated and stored in the atomic calculation. Since the atomic problem is spherically symmetric, all of the atomic matrix elements are diagonal in the m_i and m_j quantum numbers and can be evaluated as radial integrals. In order to analyze the necessary matrix elements for the full problem, it is helpful to decompose the difference Hamiltonian matrix elements D^a_{ij} into the following terms:

$$D^a_{ij} = K^a_{ij} + \langle\phi^a_i|v^a_{\mathrm{ion}}|\phi^a_j\rangle - \langle\tilde{\phi}^a_i|\tilde{v}^a_{\mathrm{loc}}|\tilde{\phi}^a_j\rangle - \langle\tilde{\phi}^a_i|\hat{v}^a|\tilde{\phi}^a_j\rangle + [\tilde{v}^a_{\mathrm{core}}]_{ij} + [V^a_H]_{ij} + [v^a_0]_{ij} + [V^a_{\mathrm{XC}}]_{ij}, \tag{A8}$$

which will be defined below.

The O^a_{ij} $[K^a]_{ij}$, $\langle\phi^a_i|v^a_{\mathrm{ion}}|\phi^a_j\rangle$, and $\langle\tilde{\phi}^a_i|\tilde{v}^a_{\mathrm{loc}}|\tilde{\phi}^a_j\rangle$ matrix elements are diagonal in the l_i and l_j quantum numbers. The overlap matrix elements (27) depend on the integrals:

$$O^a_{ij} = \delta_{l_i l_j}\delta_{m_i m_j}O^a_{n_i l_i\, n_j l_j},$$

where

$$O^a_{n_i l_i\, n_j l_j} \equiv \int_0^{r^a_c} dr[\phi^a_{n_i l_i}(r)\phi^a_{n_j l_j}(r) - \tilde{\phi}^a_{n_i l_i}(r)\tilde{\phi}^a_{n_j l_j}(r)]. \tag{A9}$$

The kinetic energy matrix elements (A8) depend on the integrals:

$$K^a_{ij} = \delta_{l_i l_j}\delta_{m_i m_j}K^a_{n_i l_i\, n_j l_j},$$

where

$$K^a_{n_i l_i\, n_j l_j} \equiv \left(-\frac{\hbar^2}{2m}\right)\int_0^{r^a_c} dr\left[\phi^a_{n_i l_i}(r)\left(\frac{d^2}{dr^2} - \frac{l_j(l_j+1)}{r^2}\right)\phi^a_{n_j l_j}(r) - \tilde{\phi}^a_{n_i l_i}(r)\left(\frac{d^2}{dr^2} - \frac{l_j(l_j+1)}{r^2}\right)\tilde{\phi}^a_{n_j l_j}(r)\right]. \tag{A10}$$

The AE ionic potential (15) matrix element is given by

$$\langle\phi^a_i|v^a_{\mathrm{ion}}|\phi^a_j\rangle = \delta_{l_i l_j}\delta_{m_i m_j}[v^a_{\mathrm{ion}}]_{n_i l_i\, n_j l_j},$$

where

$$[v^a_{\mathrm{ion}}]_{n_i l_i\, n_j l_j} \equiv \int_0^{r^a_c} dr\ \phi^a_{n_i l_i}(r)v^a_{\mathrm{ion}}(r)\phi^a_{n_j l_j}(r). \tag{A11}$$

The matrix element of the arbitrary localized potential is given by

$$\langle\tilde{\phi}^a_i|\tilde{v}^a_{\mathrm{loc}}|\tilde{\phi}^a_j\rangle = \delta_{l_i l_j}\delta_{m_i m_j}[\tilde{v}^a_{\mathrm{loc}}]_{n_i l_i\, n_j l_j},$$

where

$$[\tilde{v}^a_{\mathrm{loc}}]_{n_i l_i\, n_j l_j} \equiv \int_0^{r^a_c} dr\ \tilde{\phi}^a_{n_i l_i}(r)\tilde{v}^a_{\mathrm{loc}}(r)\tilde{\phi}^a_{n_j l_j}(r). \tag{A12}$$

The remaining Hamiltonian matrix elements are not diagonal in l_i and l_j. It is useful to define intermediate matrix elements which depend upon a ''total'' angular momentum L, where $|l_i - l_j| \leq L \leq (l_i + l_j)$. For example, the Lth moment of the density matrix element:

$$n^{aL}_{n_i l_i n_j l_j} \equiv \int_0^{r^a_c} dr\ r^L[\phi^a_{n_i l_i}(r)\phi^a_{n_j l_j}(r) - \tilde{\phi}^a_{n_i l_i}(r)\tilde{\phi}^a_{n_j l_j}(r)] \tag{A13}$$

is used in calculating the moments of the compensation charge (17). The radial part of the electrostatic potential corresponding to the Gaussian form (19)

$$\hat{v}^a_L(r) \equiv \frac{4\pi e^2}{2L+1}\left[\frac{1}{r^{L+1}}\int_0^r dr'\ r'^{L+2}g^a_L(r') + r^L\int_r^\infty dr'\ r'^{1-L}g^a_L(r')\right], \tag{A14}$$

can be evaluated analytically. In principle, this integral should be confined within the atomic sphere, but because of the localization of the Gaussian function, the integral can be extended to infinity. The first few functions are

$$\hat{v}_0^a(r) = \frac{\sqrt{4\pi}e^2}{\sigma_a}\frac{\mathrm{erf}(r/\sigma_a)}{r/\sigma_a},$$

$$\hat{v}_1^a(r) = \frac{\sqrt{4\pi}e^2}{3\sigma_a^2}\left(\frac{\mathrm{erf}(r/\sigma_a)}{(r/\sigma_a)^2} - \frac{2}{\sqrt{\pi}}\frac{e^{-(r/\sigma_a)^2}}{(r/\sigma_a)}\right),$$

$$\hat{v}_2^a(r) = \frac{\sqrt{4\pi}e^2}{5\sigma_a^3}\left[\frac{\mathrm{erf}(r/\sigma_a)}{(r/\sigma_a)^3} - \frac{2}{3\sqrt{\pi}}e^{-(r/\sigma_a)^2}\left(2+\frac{3}{(r/\sigma_a)^2}\right)\right]. \quad \text{(A15)}$$

Then, the matrix elements involving the compensation charge potential depend upon

$$\hat{v}^{aL}_{n_il_in_jl_j} \equiv \int_0^{r_c^a} dr\ \widetilde{\phi}^a_{n_il_i}(r)\hat{v}^a_L(r)\widetilde{\phi}^a_{n_jl_j}(r). \quad \text{(A16)}$$

Finally, the matrix elements of the Hartree potential, $[V_H^a]_{ij}$, depend on the four-index matrix elements:

$$V^{aL}_{n_il_in_jl_j;n_kl_kn_ll_l} \equiv \frac{4\pi e^2}{2L+1}\int_0^{r_c^a}dr\ \int_0^{r_c^a}dr'\frac{r_<^L}{r_>^{L+1}} \times[\phi^a_{n_il_i}(r)\phi^a_{n_jl_j}(r)\phi^a_{n_kl_k}(r')\phi^a_{n_ll_l}(r') - \widetilde{\phi}^a_{n_il_i}(r)\widetilde{\phi}^a_{n_jl_j}(r)\widetilde{\phi}^a_{n_kl_k}(r')\widetilde{\phi}^a_{n_ll_l}(r')]. \quad \text{(A17)}$$

In summary, the following radial matrix elements are calculated and stored in the atomic calculation for each atom of the extended system: $\{O^a_{n_il_i\,n_jl_j}\}$, $\{K^a_{n_il_i\,n_jl_j}\}$, $\{[v^a_{\mathrm{ion}}]_{n_il_i\,n_jl_j}\}$, $\{[\widetilde{v}^a_{\mathrm{loc}}]_{n_il_i\,n_jl_j}\}$, $\{[\widetilde{v}^a_{\mathrm{core}}]_{n_il_i\,n_jl_j}\}$, $\{n^{aL}_{n_il_in_jl_j}\}$, $\{\hat{v}^{aL}_{n_il_in_jl_j}\}$, and $\{V^{aL}_{n_il_in_jl_j;n_kl_kn_ll_l}\}$.

In order to evaluate the last five contributions to Eq. (A8), it is necessary to introduce intermediate quantities which depend upon the angular variables of the problem. The ''Gaunt''[37] coefficients are defined to be

$$G^{LM}_{l_im_i\,l_jm_j} \equiv \sqrt{4\pi}\int d\Omega\ Y^*_{l_im_i}(\hat{\mathbf{r}})\ Y^*_{LM}(\hat{\mathbf{r}})\ Y_{l_jm_j}(\hat{\mathbf{r}}). \quad \text{(A18)}$$

These coefficients are nonzero only when $M=m_j-m_i$.

It is also useful to define projected occupation coefficients according to the definition

$$W^a_{ij} \equiv \sum_{n\mathbf{k}} f_{n\mathbf{k}}\langle\widetilde{\Psi}_{n\mathbf{k}}|\widetilde{p}^a_i\rangle\langle\widetilde{p}^a_j|\widetilde{\Psi}_{n\mathbf{k}}\rangle. \quad \text{(A19)}$$

In order to evaluate these coefficients it is necessary to calculate the projector overlap matrix elements $\langle\widetilde{p}^a_i|\widetilde{\Psi}_{n\mathbf{k}}\rangle$. These can then be evaluated as a sum over plane-wave coefficients:

$$\langle\widetilde{p}^a_i|\widetilde{\Psi}_{n\mathbf{k}}\rangle = \sqrt{\frac{1}{\mathcal{V}}}\sum_{\mathbf{G}}\ (4\pi i^{l_i}Y^*_{l_im_i}(\widehat{\mathbf{k}+\mathbf{G}})e^{i(\mathbf{k}+\mathbf{G})\cdot\mathbf{R}^a} \times\tilde{\bar{p}}_{n_il_i}(|\mathbf{k}+\mathbf{G}|))\ A_{n\mathbf{k}}(\mathbf{G}), \quad \text{(A20)}$$

where the Fourier transform of the radial part of the projector function in the above equation is given by

$$\tilde{\bar{p}}_{n_il_i}(q) = \int_0^{r_c^a} dr\, r\ \widetilde{p}_{n_il_i}(r)j_{l_i}(qr). \quad \text{(A21)}$$

In terms of the angular and radial matrix elements defined above, the multipole moments of the compensation charge (17) can be calculated from

$$Q^a_{LM} = (-Z^a + Q^a_{\mathrm{core}})\,\delta_{L0}\delta_{M0} + \sum_{i,j}\ W^a_{ij}G^{LM}_{l_im_i\,l_jm_j}n^{aL}_{n_il_in_jl_j}. \quad \text{(A22)}$$

From a knowledge of these multipole coefficients, the fourth term of Eq. (A8) can be calculated according to

$$\langle\widetilde{\phi}^a_i|\hat{v}^a|\widetilde{\phi}^a_j\rangle = \sum_{LM}\ Q^a_{LM}\ (-1)^M G^{L\ -M}_{l_im_i\ l_jm_j}\hat{v}^{aL}_{n_il_in_jl_j}. \quad \text{(A23)}$$

The fifth (core tail) term of Eq. (A8) involves contributions from both the AE and PS matrix elements:

$$[\widetilde{v}^a_{\mathrm{core}}]_{ij} \equiv \frac{4\pi e^2}{\mathcal{V}}\sum_{\mathbf{G}\neq 0}\frac{\tilde{\bar{n}}_{\mathrm{core}}(\mathbf{G})}{G^2}\,e^{i\mathbf{G}\cdot\mathbf{R}^a} \times\sum_{LM}\ G^{LM}_{l_im_i\ l_jm_j}i^L\sqrt{4\pi}Y_{LM}(\hat{\mathbf{G}})J^{aL}_{n_il_in_jl_j}(G). \quad \text{(A24)}$$

This term does not depend upon the self-consistent valence density and is designed to converge rapidly with G. The radial Fourier integrals used in this equation are defined by

$$J^{aL}_{n_il_in_jl_j}(G) \equiv \int_0^{r_c^a} dr\ j_L(Gr)[\phi^a_{n_il_i}(r)\phi^a_{n_jl_j}(r) - \widetilde{\phi}^a_{n_il_i}(r)\widetilde{\phi}^a_{n_jl_j}(r)]. \quad \text{(A25)}$$

The sixth (Hartree) term of Eq. (A8) can be calculated according to

$$[V^a_H]_{ij} = \sum_{LM,(k,l)}\ (-1)^M G^{L\ -M}_{l_im_i\ l_jm_j}G^{LM}_{l_km_k\ l_lm_l} \times W^a_{kl}\ \ V^{aL}_{n_il_in_jl_j;n_kl_kn_ll_l}. \quad \text{(A26)}$$

In this equation, the sum over L and l_k and l_l is restricted by $|l_k-l_l|\leq L\leq l_k+l_l$ and $|l_i-l_j|\leq L\leq l_i+l_j$. The sum over m_k and m_l is restricted by $M=m_j-m_i=m_k-m_l$.

The Coulomb shift term of Eq. (A8) formally comes from the variation of the energy with respect to the multipole moment contributions which can be written[1]

$$[v^a_0]_{ij} = \sum_{LM}\ \frac{\partial E}{\partial Q^a_{LM}}\,G^{LM}_{l_im_i\ l_jm_j}n^{aL}_{n_il_in_jl_j} - \delta_{l_il_j}\delta_{m_im_j}\frac{4\pi e^2\tilde{\bar{n}}_{\mathrm{core}}(0)n^{a2}_{n_il_in_jl_i}}{6\mathcal{V}}. \quad \text{(A27)}$$

The coefficients $\partial E/\partial Q^a_{LM}$ have several contributions which can be written

$$\frac{\partial E}{\partial Q^a_{LM}} = \frac{4\pi e^2}{\mathcal{V}} \sum_{\mathbf{G}\neq 0} \frac{[\tilde{\bar{n}}(\mathbf{G}) + \overline{\hat{n}}(\mathbf{G})]^*}{G^2} Y_{LM}(\hat{\mathbf{G}})\ e^{-i\mathbf{G}\cdot\mathbf{R^a}}\ \overline{g^a_L}(G)$$
$$- \sum_{i,j}\ W^a_{ij}\ (-1)^M G^{L-M}_{l_i m_i\, l_j m_j}\ \hat{v}^{aL}_{n_i l_i n_j l_j}$$
$$- e^2 \sqrt{\frac{2}{\pi}} \frac{Q^{a\,*}_{LM}}{(2L+1)(2L+1)!!\,\sigma_a^{2L+1}}$$
$$+ \delta_{L0}\delta_{M0} \frac{4\pi e^2 \tilde{\bar{n}}_{\rm core}(0)\sigma_a^2}{4\mathcal{V}}. \qquad \text{(A28)}$$

The last term of the two equations above come from the $\mathbf{G}=\mathbf{0}$ energy term discussed below

In order to evaluate the exchange-correlation contributions to the matrix elements [last term of Eq. (A8)] it is convenient to perform the integration using a numerical grid based on a product of angular and radial points. The angular points were distributed according to Gauss-Legendre quadrature for the $\cos(\theta)$ variable and uniformly for the φ variable, with 12 quadrature points for each (in order to accurately represent integrals for basis functions with $l\leqslant 3$). The radial points were chosen to be the same as those used in the radial integration in the atomic program. Denoting each angular integration mesh point by $\hat{\mathbf{r}}_\alpha$, and its corresponding integration weight by w_α (where $\Sigma_\alpha w_\alpha = 4\pi$), the matrix element can be evaluated according to

$$[V^a_{\rm XC}]_{ij} = \sum_\alpha\ w_\alpha Y^*_{l_i m_i}(\hat{\mathbf{r}}_\alpha) Y_{l_j m_j}(\hat{\mathbf{r}}_\alpha)$$
$$\times \int_0^{r_c^a} dr \{\mu_{\rm xc}[n^a(\hat{\mathbf{r}}_\alpha r) + n^a_{\rm core}(r) - \tilde{n}^a_{\rm core}(r)$$
$$+ \tilde{n}_{\rm core}(\hat{\mathbf{r}}_\alpha r)]\phi^a_{n_i l_i}(r)\phi^a_{n_j l_j}(r)$$
$$- \mu_{\rm xc}[\tilde{n}^a(\hat{\mathbf{r}}_\alpha r) + \tilde{n}_{\rm core}(\hat{\mathbf{r}}_\alpha r)]\tilde{\phi}^a_{n_i l_i}(r)\tilde{\phi}^a_{n_j l_j}(r)\}, \qquad \text{(A29)}$$

where the radial integral over r is performed for each angular mesh point $\hat{\mathbf{r}}_\alpha$. The efficiency of evaluating (A29) can be improved by separating the angular and radial contributions in the atomic density functions (6) and (7) according to

$$n^a(\hat{\mathbf{r}}_\alpha r) = \sum_{i,j}\ W^a_{ij} Y^*_{l_i m_i}(\hat{\mathbf{r}}_\alpha) Y_{l_j m_j}(\hat{\mathbf{r}}_\alpha) \frac{\phi^a_{n_i l_i}(r)\phi^a_{n_j l_j}(r)}{r^2},$$

and

$$\tilde{n}^a(\hat{\mathbf{r}}_\alpha r) = \sum_{i,j}\ W^a_{ij} Y^*_{l_i m_i}(\hat{\mathbf{r}}_\alpha) Y_{l_j m_j}(\hat{\mathbf{r}}_\alpha)\ \frac{\tilde{\phi}^a_{n_i l_i}(r)\tilde{\phi}^a_{n_j l_j}(r)}{r^2}. \qquad \text{(A30)}$$

The PAW atomic matrix elements that are needed to evaluate the Hamiltonian can also be used to evaluate the total valence energy (8). The ''one-center'' contributions are given by

$$E^a - \tilde{E}^a = \sum_{i,j}\ W^a_{ij}\Big[\delta_{l_i l_j}\delta_{m_i m_j}(K^a_{n_i l_i n_j l_j} + [v^a_{\rm ion}]_{n_i l_i n_j l_j}$$
$$- [\tilde{v}^a_{\rm loc}]_{n_i l_i n_j l_j}) - \langle\tilde{\phi}^a_i|\hat{v}^a|\tilde{\phi}^a_j\rangle + [\tilde{v}^a_{\rm core}]_{ij}$$
$$+ \frac{1}{2}[V^a_H]_{ij}\Big] - \hat{E}^a - \tilde{E}^a_{\rm core} - \tilde{E}^{a0}_{\rm core}$$
$$+ (E_{\rm xc}[n^a + n^a_{\rm core} - \tilde{n}^a_{\rm core} + \tilde{n}_{\rm core}] - E_{\rm xc}[n^a_{\rm core}]$$
$$- E_{\rm xc}[\tilde{n}^a + \tilde{n}_{\rm core}]). \qquad \text{(A31)}$$

The self-Coulomb repulsion of the compensation charge has the analytic form:

$$\hat{E}^a = \frac{e^2}{2}\sqrt{\frac{2}{\pi}}\ \sum_{LM}\ \frac{|Q^a_{LM}|^2}{(2L+1)(2L+1)!!\,\sigma_a^{2L+1}}. \qquad \text{(A32)}$$

The core energy contribution can be evaluated according to

$$-\tilde{E}^a_{\rm core} = \frac{4\pi e^2}{\mathcal{V}} \sum_{\mathbf{G}\neq 0} \frac{\tilde{\bar{n}}_{\rm core}(\mathbf{G})}{G^2} e^{i\mathbf{G}\cdot\mathbf{R}^a}$$
$$\times \int_0^{r_c^a} dr\ 4\pi r^2 n^a_{\rm ion}(r) j_0(Gr) - \tilde{E}^a_{\text{self-core}}, \qquad \text{(A33)}$$

where

$$\tilde{E}^a_{\text{self-core}} \equiv e^2 \int\ d^3r\ \frac{n^a_{\rm ion}(r)\tilde{n}^a_{\rm core}(r)}{|\mathbf{r}-\mathbf{r}'|}$$
$$+ \frac{e^2}{2}\int\int\ d^3r\ d^3r' \frac{\tilde{n}^a_{\rm core}(r)\tilde{n}^a_{\rm core}(r')}{|\mathbf{r}-\mathbf{r}'|}. \qquad \text{(A34)}$$

The $\mathbf{G}=\mathbf{0}$ energy term takes the value

$$-\tilde{E}^{a0}_{\rm core} = \frac{4\pi e^2 \tilde{\bar{n}}_{\rm core}(0)}{\mathcal{V}}$$
$$\times \Big[\frac{Q^a_{00}\sigma_a^2}{4} - \frac{1}{6}\sum_{i,j}\ \delta_{l_i l_j}\delta_{m_i m_j} W^a_{ij} n^{a2}_{n_i l_i n_j l_i}$$
$$- \frac{1}{6}\int_0^{r_c^a} dr\ \ 4\pi r^4 [n^a_{\rm core}(r) - \tilde{n}^a_{\rm core}(r)]\Big], \qquad \text{(A35)}$$

where $n^{a2}_{n_i l_i n_j l_i}$ is defined by Eq. (A13), for each value of l_i. The exchange-correlation terms $(E_{\rm xc}[n^a + n^a_{\rm core} - \tilde{n}^a_{\rm core} + \tilde{n}_{\rm core}] - E_{\rm xc}[\tilde{n}^a + \tilde{n}_{\rm core}])$ are evaluated using a scheme similar to that used in the evaluation of the Hamiltonian contributions (A29), while $E_{xc}[n^a_{\rm core}]$ is a constant for each atom.

[1] P. E. Blöchl, Phys. Rev. B **50**, 17 953 (1994). We have attempted to follow the notation introduced in this reference.
[2] David Vanderbilt, Phys. Rev. B **41**, 7892 (1990).
[3] Peter E. Blöchl, Phys. Rev. B **41**, 5414 (1990).
[4] Chris B. Van de Walle and P. E. Blöchl, Phys. Rev. **47**, 4244 (1993).
[5] Peter Marl, Karlheinz Schwarz, and Peter E. Blöchl, J. Chem. Phys. **100**, 8194 (1994).
[6] J. Sarnthein, K. Schwarz, and P. E. Blöchl, Phys. Rev. B **53**, 9084 (1996).
[7] Steven G. Louie, Kai-Ming Ho, and Marvin L. Cohen, Phys. Rev. B **19**, 1774 (1979).
[8] P. Blaha, K. Schwarz, P. Dufek, and R. Augustyn, computer code WIEN95, Technical University of Vienna, Vienna, 1995. [Improved and updated Unix version of the original copyrighted WIEN-code, which was published by P. Blaha, K. Schwarz, P. Sorantin, and S. B. Trickey, in Comput. Phys. Commun. **59**, 399 (1990)].
[9] P. Hohenberg and W. Kohn, Phys. Rev. **136**, B864 (1964); W. Kohn and L. J. Sham, *ibid.* **140**, A1133 (1965).
[10] Robert G. Parr and Weitao Yang, *Density-Functional Theory of Atoms and Molecules* (Oxford University Press, New York, 1989).
[11] Warren E. Pickett, Comput. Phys. Rep. **9**, 115 (1989).
[12] M. C. Payne, M. P. Teter, D. C. Allan, T. A. Arias, and J. D. Joannopoulos, Rev. Mod. Phys. **64**, 1045 (1992).
[13] N. A. W. Holzwarth and Y. Zeng, Phys. Rev. B **49**, 2351 (1994).
[14] J. P. Perdew and Y. Wang, Phys. Rev. B **45**, 13 244 (1992).
[15] J. P. Perdew, J. A. Chevary, S. H. Vosko, K. A. Jackson, M. R. Pederson, D. J. Singh, and D. Fiolhais, Phys. Rev. B **46**, 6671 (1992).
[16] U. von Barth and C. D. Gelatt, Phys. Rev. B **21**, 2222 (1980).
[17] Alan F. Wright and J. S. Nelson, Phys. Rev. B **50**, 2159 (1994).
[18] Y. Zeng and N. A. W. Holzwarth, Phys. Rev. **50**, 8214 (1994); Y. Zeng (unpublished).
[19] In this manuscript, the index i is an abbreviation for the radial and angular quantum numbers $n_i l_i m_i$. The shorthand and full index notation are used interchangeably.
[20] Blöchl (Ref. 1) showed how it is possible to extend the PAW formalism to include the effects of core relaxation. However, the results of the present manuscript are strictly in the frozen core approximation.
[21] In Eq. (10) a constant energy shift due to the exchange-correlation energy of the frozen core density alone has been included for convenience.
[22] L. F. Mattheiss and D. R. Hamann, Phys. Rev. B **33**, 823 (1986).
[23] P. P. Ewald, Ann. Phys. (Leipzig) **64**, 253 (1921).
[24] J. Ihm, Alex Zunger, and Marvin L. Cohen, J. Phys. C **12**, 4409 (1979).
[25] Ernest R. Davidson, Comput. Phys. **7**, 519 (1993).
[26] Douglas R. Hartree, *The Calculation of Atomic Structures* (Wiley, New York, 1957).
[27] Frank Herman and Sherwood Skillman, *Atomic Structure Calculations* (Prentice-Hall, Englewood Cliffs, NJ, 1963).
[28] Alexander Khein, Phys. Rev. B **51**, 16 608 (1995).
[29] Xavier Gonze, Roland Stumpf, and Matthias Scheffler, Phys. Rev. B **44**, 8503 (1991); Xavier Gonze, Peter Käckell, and Matthias Scheffler, Phys. Rev. **41**, 12 264 (1990).
[30] C.-L. Fu and K.-M. Ho, Phys. Rev. B **28**, 5480 (1983).
[31] F. D. Murnaghan, Proc. Natl. Acad. Sci. U.S.A. **30**, 244 (1944).
[32] Charles Kittel, *Introduction to Solid State Physics*, Seventh ed. (Wiley, New York, 1996).
[33] Experimental results quoted in the Hartree-Fock study of M. Catti, R. Dovesi, A. Pavese, and V. R. Saunders, J. Phys. Condens. Matter **3**, 4151 (1991).
[34] Experimental results quoted in the pseudopotential study of K. J. Chang and Marvin L. Cohen, Phys. Rev. B **35**, 8196 (1987).
[35] V. L. Sliwko, P. Mohn, K. Schwarz, and P. Blaha, J. Phys. Condens. Matter **8**, 799 (1996). Slight differences in our results for Ca and V are due to our less accurate but internally consistent Brillouin zone integration technique.
[36] Renata M. Wentzcovitch and Henry Krakauer, Phys. Rev. B **42**, 4563 (1990). A different choice of LDA functional yielded different results for Ca.
[37] Manuel Rotenberg, R. Bivins, N. Metropolis, and John K. Wooten, Jr., *The 3-j and 6-j Symbols* (Technology Press, Massachusetts Institute of Technology, Cambridge, MA, 1959). The definition (A18) is slightly different from the standard.